

Reduced Complexity ML Interference-Aware Parallel and SIC Receivers for SU-MIMO Systems

Elena Lukashova, Florian Kaltenberger, Raymond Knopp

EURECOM

Campus SophiaTech, 450 Route des Chappes,
06410 Biot, France

Email: (elena.lukashova@eurecom.fr)

Abstract—Although the base station processing and the majority of the protocols of the wireless systems are standardized by 3GPP, the receiver architecture and implementation remain vendor-dependent. The receiver design should fulfill computational efficiency requirements, and be evaluated in practical simulators or emulators that are compliant with real-world wireless standards. In this paper, we provide a comparative study of two low complexity Maximum-Likelihood receivers with the Parallel Interference-Aware (PIA) detection and with the Successive Interference Canceling (SIC) detection. Given 5MHz of LTE bandwidth, the SIC receiver achieves up to 4Mbit/s throughput gain in Rician fading and 1.8Mbit/s in Rayleigh fading compared to the PIA receiver. The quantification of computational effort demonstrates short signal processing time, which makes our receivers suitable for real-time modems. Our empirical simulations deliver insights on the optimal SNR regimes and the modulation and coding schemes combinations for both codewords to maintain high level of throughput.

Keywords—Interference-Awareness, Maximum-Likelihood, Reduced Complexity, Successive Interference Canceling

I. INTRODUCTION

Over the last few years, enhancing system performance through the design of advanced receiver architectures has been extensively studied [1]. However, real-world feasibility remains the prime criterion when seeking solutions to the problem of balancing the complexity and the performance of receivers. Relatively easy to build linear receivers, such as Zero Forcing (ZF) and Minimum Mean Squared Error (MMSE), are sensitive to the number of paths in a multi-path environment and show significant performance degradation at moderate and high SNR levels [2]. At the same time, the complexity of the optimum non-linear Maximum-Likelihood (ML) receiver proliferates with the number of spatial layers and the modulation order: an exhaustive search among all possible transmitted vector candidates must be performed. The near-optimal non-linear solutions with reduced implementation complexity have become a fair compromise to balance complexity-performance trade-off. In practice, the ML detection is replaced with the maximum *a posteriori* probability (MAP) approximation [3]. However, the complexity is still high and further simplifications are required. The sub-optimal Reduced Complexity Maximum Likelihood (R-ML) receiver design was introduced to circumvent the extremely high computational complexity of the ML and MAP receivers.

The key idea behind the majority of reduced-complexity non-linear solutions consists in reducing the search space by removing unreliable candidates or selecting the most probable symbols that could have been transmitted. This concept is applied in sphere decoding and tree search detection. LTE-compatible sphere decoders and QRD-based detectors have been reported in [4], [5].

Another research direction of complexity reduction consists in manipulating the Log-Likelihood Ratio (LLR) metrics. Ghaffar and Knopp reduced one complex dimension of search without compromising performance by decoupling the real and imaginary parts of Multiple-Input-Multiple-Output (MIMO) soft bit LLR metric [6]. By being combined with the Matched Filter (MF), metrics are division-free and can therefore be easily deployed in real-time modems.

Conventional receivers treat interference as Gaussian and apply interference whitening in order to recover the transmitted signal. The interference-aware (IA) architecture of the advanced receivers bring significant gains to the system performance, even if only blind interference detection is applied [7]. Ghaffar and Knopp developed the simplified receiver design that is capable of interference mitigation through the exploitation of its structure [8]. The real-time measurements confirmed that the proposed receiver offers significant gains, which increase together with the modulation order [9].

Single-User MIMO (SU-MIMO) multi-stream IA detection falls into three groups: joint ML, R-ML Parallel Interference-Aware (PIA) and R-ML Successive Interference Canceling (R-ML SIC). Inspired by [8] and [9], we implement our PIA [10] and SIC [11] receivers in the downlink simulator of OpenAirInterface (OAI) – an open source LTE platform developed at EURECOM [12] conforming to 3GPP standards [13]–[15] with a high degree of realism and flexibility. Quantification of computational effort is performed to evaluate the practical feasibility of our receivers. Our experiments deliver insights on the optimal SNR regimes and modulation and coding schemes (MCS) combination for both codewords, which allow to maintain high level of throughput. Furthermore, we provide an information-theoretic analysis in order to define potential performance bounds. We build upon these results using mutual information outage probability concept [16] and evaluate the gap between the empirical results and the theoretical expectations.

II. SYSTEM MODEL

We consider a downlink Closed Loop Spatial Multiplexing (CLSM) Transmission Mode 4 (TM4) scenario with two codewords (CW) and $n_{\text{tx}} = 2$ transmit and $n_{\text{rx}} = 2$ receive antennas. We refer to the lower-rate R_0 CW as CW_0 , and CW_1 is always provided with equal or higher rate R_1 . The MCS are known to the UE from the Downlink Control Information (DCI). The received signal vector $\mathbf{y}_l \in \mathbb{C}^{2 \times 1}$ for the l -th subcarrier observed by the UE is given by

$$\mathbf{y}_l = \tilde{\mathbf{H}}_l \mathbf{P}_l \mathbf{x}_l + \mathbf{n}_l, \quad l = 1, 2, \dots, L, \quad (1)$$

where $\mathbf{x}_l \in Q^{M_0, M_1}$ is the vector of two complex symbols x_0 and x_1 with variance σ_0^2 and σ_1^2 , $Q^{M_0, M_1} := Q^{M_0} \times Q^{M_1}$ is the Cartesian product of two modulation alphabets Q^{M_0} and Q^{M_1} , $M_0, M_1 \in \{4, 6\}$ are the modulation orders of the QAM constellations. The vector \mathbf{n}_l is the Zero Mean Circularly Symmetric Complex Gaussian (ZMCSG) white noise of double-sided power spectral density $N_0/2$. The matrix $\tilde{\mathbf{H}}_l$ represents the 2×2 MIMO Rician channel, and is constructed in the classical manner:

$$\tilde{\mathbf{H}}_l = \underbrace{\sqrt{\frac{K}{K+1}} \begin{bmatrix} 1 & e^{-j\phi} \\ e^{j\phi} & 1 \end{bmatrix}}_{\text{LOS component}} + \underbrace{\sqrt{\frac{1}{K+1}} \mathbf{H}_l}_{\text{NLOS component}},$$

where \mathbf{H}_l is a matrix of i.i.d. ZMCSG random entries with a variance of 0.5 per dimension. A parameter ϕ is a phase-shift, strongly related to the antenna array configuration and its orientation towards the Line-of-Sight (LOS) component, and K is the Rician K-factor. A matrix \mathbf{P}_l is a codebook-based LTE precoder [14].

For the sake of simplicity, we drop the subcarrier index and replace the multiplication of $\tilde{\mathbf{H}}$ and \mathbf{P} with the effective channel \mathbf{H}_{eff} :

$$\mathbf{y} = \mathbf{H}_{\text{eff}} \mathbf{x} + \mathbf{n}, \quad \mathbf{H}_{\text{eff}} = [\mathbf{h}_{\text{eff}0} \quad \mathbf{h}_{\text{eff}1}]. \quad (2)$$

III. THE PRECODER MATRIX INDICATOR CALCULATION

The LTE precoding codebooks are standardized by 3GPP [14] for the different transmission settings, such as the transmission rank, the antenna configuration, etc. For our 2×2 system using CLSM, the eNodeB has two possible choices for the precoding matrix \mathbf{P} :

$$\mathbf{P} \in \left\{ \frac{1}{2} \begin{bmatrix} 1 & 1 \\ 1 & -1 \end{bmatrix}, \frac{1}{2} \begin{bmatrix} 1 & 1 \\ j & -j \end{bmatrix} \right\}.$$

Based on the channel measurement and estimation, the UE selects the optimal matrix and signals the corresponding precoder matrix indicator (PMI) to the eNodeB. The criterion based on maximum Mutual Information (MI) [17] is optimal, but is difficult to implement: it involves a time-consuming computation of MI or requires precomputed look-up tables. An intuitive and easy to implement solution is to maximize the SNR level of the first stream [18], since the decodability of the second CW is a function of the probability of error of the first one. In the latter case, the UE computes two ratios

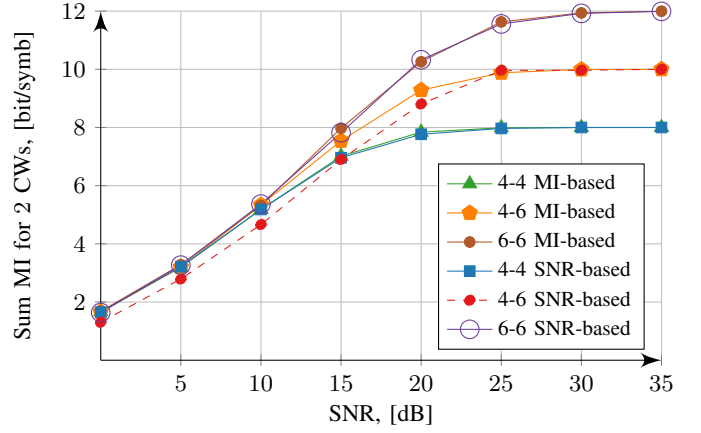


Figure 1: Potential mutual information levels for two codewords using our R-ML SIC receiver with MI-based and SNR-based precoder selection for the CWs with the modulation orders $M_0, M_1 \in \{4, 6\}$ between the SNR values of the first stream and the second stream:

$$\left(\frac{\|\mathbf{h}_0 + \mathbf{h}_1\|^2}{\|\mathbf{h}_0 - \mathbf{h}_1\|^2}, \frac{\|\mathbf{h}_0 + j\mathbf{h}_1\|^2}{\|\mathbf{h}_0 - j\mathbf{h}_1\|^2} \right). \quad (3)$$

If the first ratio is bigger than the second one, then the UE selects the precoder matrix with real values, otherwise with complex values. This computation can be simplified to the evaluation of the real and imaginary parts of the correlation coefficient $\rho_{10} = \mathbf{h}_{\text{eff}1}^H \mathbf{h}_{\text{eff}0}$ (the derivation can be found in Appendix):

$$\mathbf{P} = \begin{cases} \frac{1}{2} \begin{bmatrix} 1 & 1 \\ 1 & -1 \end{bmatrix}, & \text{for } \Re(\rho_{10}) \geq \Im(\rho_{10}); \\ \frac{1}{2} \begin{bmatrix} 1 & 1 \\ j & -j \end{bmatrix}, & \text{for } \Re(\rho_{10}) < \Im(\rho_{10}). \end{cases}$$

To compare two criteria, we perform a numerical analysis of the potential performance loss. For the MI-based criterion, the mutual information for both precoders is estimated and the UE selects the precoder that corresponds to the highest mutual information. As we see in Fig. 1, the MI-based criterion outperforms the suboptimal SNR-based computation only when CW_0 is mapped on 16QAM constellation, and CW_1 belongs to 64QAM. However, this gap vanishes when both codewords belong to the same constellation. The SNR-based precoder selection thus is a light-weight solution and promises performance levels that are close to optimal MI criterion.

IV. RECEIVER ARCHITECTURE

A. Common R-ML IA Blocks

The signal processing of downlink data starts with the linear MF operation, common to both PIA and SIC receivers. The MIMO demodulator passes the received signal \mathbf{y} (2) through linear MF operation, transforming the received signal into

$$\mathbf{y}_{\text{MF}} = \mathbf{H}_{\text{eff}}^H \mathbf{y}. \quad (4)$$

After MF, both PIA and SIC receivers provide an identical treatment to the lower-rate CW_0 by calculating LLR_0 using the

$$I(X_0; \mathbf{Y}_{MF} | \mathbf{H}_{\text{eff}}, M_0, M_1, N_0) = \log M_0 - \frac{1}{M_0 M_1 N_n} \left(\sum_{x_0 \in Q^{M_0}} \sum_{x_1 \in Q^{M_1}} \sum_z^{N_n} \log \frac{\sum_{x'_0 \in Q^{M_0}} \sum_{x'_1 \in Q^{M_1}} \exp \left[-\frac{1}{N_0} \|\mathbf{y}_{MF} - \mathbf{h}_0 x'_0 - \mathbf{h}_1 x'_1\|^2 \right]}{\sum_{x''_1 \in Q^{M_1}} \exp \left[-\frac{1}{N_0} \|\mathbf{y}_{MF} - \mathbf{h}_0 x_0 - \mathbf{h}_1 x''_1\|^2 \right]} \right), \quad (8)$$

$$I(X_1; \mathbf{Y}_{MF} | X_0, \mathbf{H}_{\text{eff}}, M_0, M_1, N_0) = \log M_1 - \frac{1}{M_0 M_1 N_n} \left(\sum_{x_0 \in Q^{M_0}} \sum_{x_1 \in Q^{M_1}} \sum_z^{N_n} \log \frac{\sum_{x'_1 \in Q^{M_1}} \exp \left[-\frac{1}{N_0} \|\mathbf{y}_{MF} - \mathbf{h}_0 x_0 - \mathbf{h}_1 x'_1\|^2 \right]}{\exp \left[-\frac{1}{N_0} \|\mathbf{y}_{MF} - \mathbf{h}_0 x_0 - \mathbf{h}_1 x_1\|^2 \right]} \right). \quad (9)$$

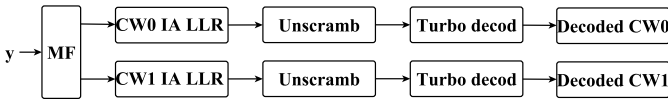


Figure 2: R-ML PIA receiver scheme. Both codewords are handled in the same manner using interference-aware low-complexity bit metrics.

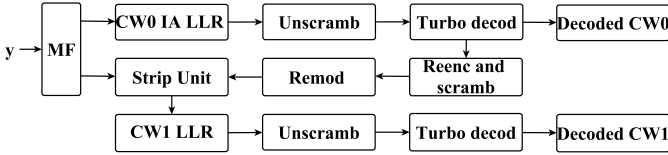


Figure 3: R-ML SIC receiver scheme. The first codeword receives treatment identical to the PIA receiver, while the second codeword undergoes the SIC procedure.

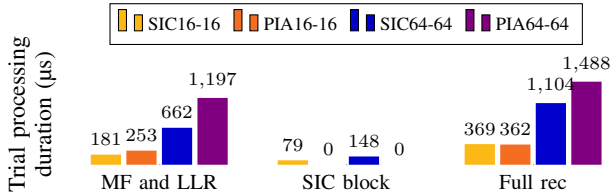


Figure 4: Time consumed by MF and LLR, and SIC blocks of our SIC and PIA receivers to process downlink data.

IA bit metric $M_0_M_1_llr$ [6], which treats CW_1 as interference. The soft LLR values are then fed to the unscrambling procedure and consequently to the turbo decoder.

If CW_0 is decoded correctly, the UE forms the acknowledging message ACK_0 to confirm successful decoding to the eNodeB. Following this scenario, the SIC receiver triggers the SIC procedure. However, if CW_0 is not decoded, no attempt is made to decode CW_1 .

The PIA receiver acts differently (Fig. 2): the LLR values for CW_0 and CW_1 are computed in parallel using the $M_0_M_1_llr$ and $M_1_M_0_llr$ functions [6], and fed to two turbo decoders. The probability of CW_1 to be successfully decoded does not depend on the decodability of CW_0 .

B. SIC Procedure

The SIC procedure starts with re-encoding the recently decoded sequence of bits of CW_0 and mapping them onto modulation symbols x_0 (Fig. 3). The compensated received signal on the second antenna is seen as

$$y_{MF_1} = \rho^* x_0 + (h_{\text{eff}01}^* h_{\text{eff}01} + h_{\text{eff}11}^* h_{\text{eff}11}) x_1 + n'_1.$$

After multiplication of x_0 , obtained from the successful decoding of CW_0 , with correlation coefficient ρ^* and subtraction

the result from y_{MF_1} , x_1 enjoys interference-free detection:

$$\tilde{y}_{MF_1} = (h_{\text{eff}01}^* h_{\text{eff}01} + h_{\text{eff}11}^* h_{\text{eff}11}) x_1 + n'_1.$$

The LLR values for CW_1 decoding now can be computed with the light-weight M_1_llr interference-free bit metric [6].

C. Computational Complexity

To be practically feasible for real-time transmissions, the receiver design has to be computationally efficient. In the real LTE modem, the ACK/NACK report must be generated in the third subframe after the data reception, giving a 2 ms window to process the data. Using real-time measurements, we verify that our receivers satisfy this requirement. The measurements are performed using one thread of the 64-bit machine with 2.10 GHz processor and 8 GB of memory.

The measurements take into account the MF and LLR computations, unscrambling, SIC block and decoding. The frame processing duration is averaged among 10000 frames. For 16QAM, both receivers take an equal amount of time to process the data (Fig. 4). This means that for 16QAM-16QAM the SIC block takes approximately the same time as the IA LLR metric for CW_1 in PIA detection. For 64QAM-64QAM the SIC receiver is 300 μs faster thanks to the SIC block that takes less time than the 64-64QAM IA LLR metric for the CW_1 . This means that for high modulation order the SIC receiver is 25% more time efficient. Both our receivers take less than 1.5 ms to process 1 downlink frame in 5 MHz bandwidth, and thus can be deployed in real systems. For the higher bandwidth we propose to use multi-threading.

V. MUTUAL INFORMATION ANALYSIS

Before we present the results of the practical simulations performed in our downlink simulator, we investigate the theoretical potential of our SIC and PIA receivers. The MI analysis provides the theoretical expectation of the achievable performance under the idealistic assumption of an infinite block length and zero outage. For the practical LTE system with finite discrete alphabets, there is no closed form expression for MI. However, it can be numerically approximated via Monte-Carlo simulations. Following the MI chain rule, the total MI of the MIMO system with joint I_{ML} ML decoding can be decomposed into I_0 and I_1 without compromising the performance:

$$I(X_0, X_1; \mathbf{Y} | \mathbf{H}_{\text{eff}}, M_0, M_1, N_0) = \underbrace{I(X_0; \mathbf{Y}_{MF} | \mathbf{H}_{\text{eff}}, M_0, M_1, N_0)}_{I_{\text{SIC}}=I_{\text{ML}}} + \underbrace{I(X_1; \mathbf{Y}_{MF} | X_0, \mathbf{H}_{\text{eff}}, M_0, M_1, N_0)}_{I_1}.$$

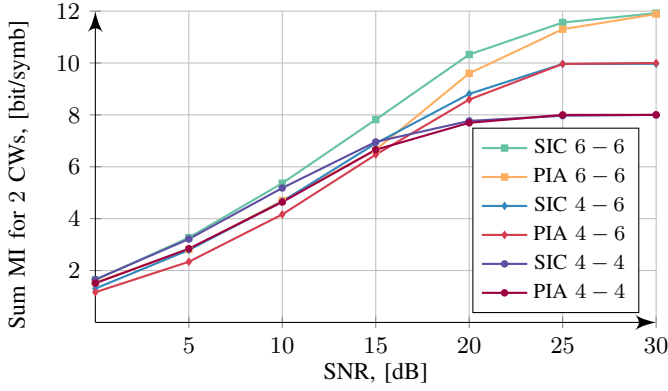


Figure 5: MI potential for SIC and PIA receivers in Rayleigh fading for the CWs with the modulation orders $M_0, M_1 \in \{4, 6\}$.

The value of MI I_0 between the received signal \mathbf{Y}_{MF} and the transmitted symbol X_0 can be computed using (8) [8] and corresponds to the MI of CW_0 for both the SIC and the PIA receivers. The value of the conditional MI I_1 between \mathbf{Y}_{MF} and the transmitted symbol X_1 given the knowledge of symbol X_0 can be approximated using (9) [8], and corresponds to the interference-free detection of CW_1 . The PIA receiver knows the modulation order of CW_0 from the DCI, but does not possess a precise information about X_0 :

$$\underbrace{I(X_0, X_1; \mathbf{Y} | \mathbf{H}_{\text{eff}}, M_0, M_1, N_0)}_{I_{\text{PIA}}} = \underbrace{I(X_0; \mathbf{Y}_{MF} | \mathbf{H}_{\text{eff}}, M_0, M_1, N_0)}_{I_0} + \underbrace{I(X_1; \mathbf{Y}_{MF} | \mathbf{H}_{\text{eff}}, M_0, M_1, N_0)}_{I_{\text{PIA}}}.$$

The first CW demonstrates identical levels of MI in PIA and SIC receivers. However, it is not the case for CW_1 , since CW_1 enjoys interference-free detection with the SIC receiver and thus achieves higher MI than CW_1 with the PIA detection at the same SNR level. This results in overall higher MI levels for the SIC receiver, as proved with the numerical simulations in Fig. 5.

The MI analysis provides the number of fundings. The 16QAM-16QAM modulation is preferable for low SNR regimes, as in this regime it guarantees performance level very close to 64QAM-64QAM (Fig. 5), while the computational time is significantly reduced, as we saw in previous section in Fig. 4. While 64QAM-64QAM strongly outperforms other combinations of the modulation orders in moderate and high SNR levels, the 16QAM-64QAM scenario has a narrow region of application since the MI of CW_0 is a function of the constellation size of CW_1 and thus tends to decrease as the modulation order of CW_1 increases.

VI. PRACTICAL RESULTS

We examine the empirical throughput, that is obtained as a result of the link-level simulations (LLS) using OAI [12] downlink simulator. The simulator provides the flexibility to vary the LTE transmission parameters as well as to customize the propagation environment.

A. Simulation Parameters

The simulations were performed for Rayleigh and Rician flat fading channels. For the Rician channel, Angle-of-Arrival (AoA) $\alpha = \frac{\pi}{4}$ radians and K-factor of 9.5 dB were chosen. Given 5MHz of LTE bandwidth (25 Resource Blocks), 3000 packets with 1 Physical Downlink Control Channel (PDCCH) symbol were transmitted over the wide range of noise variances. The transmission of two spatially multiplexed codewords was performed using a 2×2 antenna configuration. We chose $10 \leq \text{MCS}_0 \leq \text{MCS}_1 \leq 28$, BLER of 10^{-2} and applied perfect channel estimation at the UE.

B. Empirical Throughput and MCS Optimization

In a real LTE system, the throughput is limited by the rate R defined by the MCS [13]. SIC receivers are sensitive to the choice of MCS: if the instantaneous channel does not support the rate of MCS_0 , CW_0 is not decoded and the SIC procedure is thus not triggered. On the other hand, if the first stream is decoded, the second stream becomes interference-free and can potentially carry higher information rates. The PIA detection is less sensitive to the non-optimal MCS choice, since the probabilities of the successful decoding do not hold a direct dependency between each other.

We aim to define the optimal MCS_0^* and MCS_1^* that maximize the throughput for our receivers in different SNR regimes by applying a brute force search method to the previously computed traces of the LLS. The traces contain per-stream and total throughputs averaged across the channel realizations for a wide range of SNR values for all MCS combinations. The values of throughput are computed based on the Block Error Rate statistics delivered by our simulator for each SNR point. Unlike with the PIA receiver, where the MCS choice on the streams is independent from each other, with the SIC receiver the decodability of the second stream is a function of BLER of the first stream, and we thus want to define an optimal *combination of the MCS*.

For each SNR point, we choose the values of $R_0^*(\text{SNR})$ and $R_1^*(\text{SNR})$ that provide the maximum throughput $T_{\text{tot,sim}}^*(R_0^*(\text{SNR}), R_1^*(\text{SNR}), \text{SNR})$. The empirically optimized throughput for our SIC receiver in Rayleigh channel is illustrated in Fig. 6. The solid lines represent the throughput $T_{\text{tot,sim}}(R_0, R_1, \text{SNR})$ obtained for all possible MCS combinations for CW_0 and CW_1 , and the red circles mark the optimized throughput $T_{\text{tot,sim}}^*(R_0^*, R_1^*, \text{SNR})$, which is an envelope of the family of the solid lines. Our experiments have proved that, thanks to the interference-free detection, the SIC receiver supports higher MCS for the second codeword, while for the PIA receiver the MCS values for both streams remain at approximately same level.

Fig. 7 illustrates the optimized throughput $T_{\text{tot,sim}}^*$ for the SIC receiver and PIA receivers in Rician and Rayleigh fading environment. The SIC receiver gains up to 4 Mbit/s in moderate and high SNR regime, while in the Rayleigh channel this gap is not so significant and achieves 1.5Mbit/s. The SNR penalty for non-perfect channel estimation (Least Squares) is 1.5-2dB.

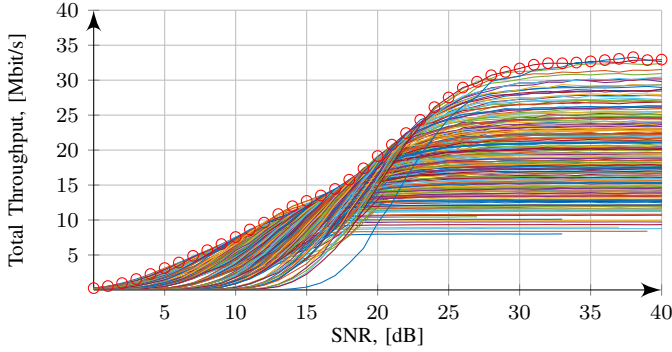


Figure 6: Optimized practically achieved throughput for our SIC receiver in Rayleigh channel with perfect channel estimation. The solid lines represent the empirical throughput $T_{\text{tot,sim}}$, obtained for all possible MCS combinations for both codewords, and the red circles mark the optimized throughput $T_{\text{tot,sim}}^*$, which is an envelope of the family of the solid lines.

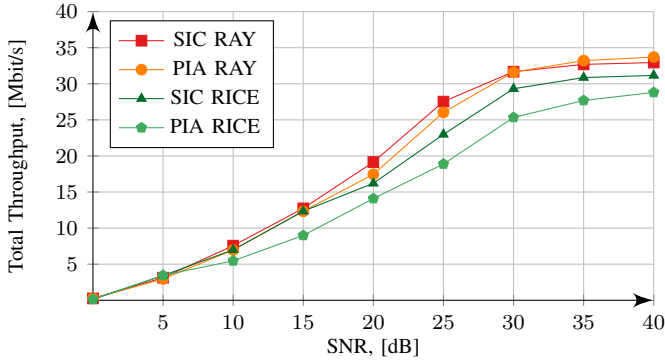


Figure 7: The optimized throughput $T_{\text{tot,sim}}^*$ for the SIC and PIA receivers in Rayleigh and Rician fading environment and with perfect channel estimation.

VII. PRACTICE VS THEORETICAL EXPECTATIONS

To quantify how much the results from our LLS are affected by the receiver imperfections, round-off errors, and fixed point implementation, we perform a comparison between the empirical throughput and the theoretical expectations delivered by the MI analysis under the idealistic assumptions in Section V.

To bring the theoretical expectations together with the empirical results, we apply a concept of *mutual information outage probability* [16]. This allows to take into account the events where the capacity of the channel (in LTE systems with Bit Interleaved Coded Modulation represented by MI) is lower than the rate of the MCS currently being used. In this analysis, we consider our SIC receiver, and the results for the PIA detection can be derived in the similar way.

The probabilities of outage for CW_0 and CW_1 using SIC receiver are defined respectively as:

$$P_{\text{out}_0}(R_0, \text{SNR}) = \Pr(I_0(\mathbf{H}_{\text{eff}}, \text{SNR}) < R_0),$$

$$P'_{\text{out}_1}(R_0, R_1, \text{SNR}) = P_{\text{out}_0}(R_0, \text{SNR})P_{\text{out}_1}(R_1, \text{SNR}).$$

Similarly, $P_{\text{out}_1}(R_1, \text{SNR}) = \Pr(I_1(\mathbf{H}_{\text{eff}}, \text{SNR}) < R_1)$, and the MI values for the first and second codeword $I_0(\mathbf{H}_{\text{eff}}, \text{SNR})$ and $I_1(\mathbf{H}_{\text{eff}}, \text{SNR})$ can be approximated using (8) and (9). Let

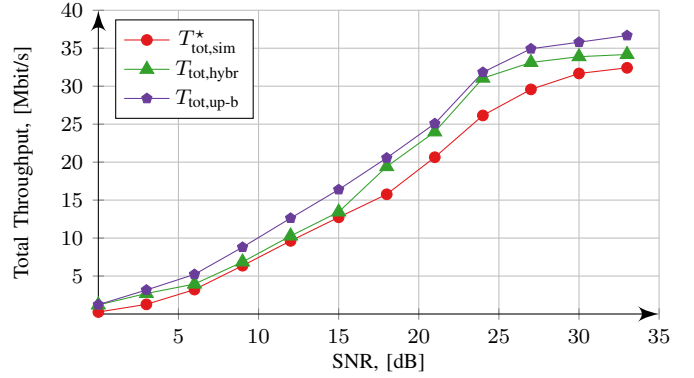


Figure 8: Empirical, Hybrid and Upper-Bound throughput for our SIC receiver in the Rayleigh channel.

the throughput $T_{\text{tot}}(R_0, R_1, \text{SNR})$ be the total throughput of our 2×2 system with SIC detection, then

$$T_{\text{tot}}(R_0, R_1, \text{SNR}) = R_0(1 - P_{\text{out}_0}(R_0, \text{SNR})) + R_1(1 - P_{\text{out}_0}(R_0, \text{SNR}))(1 - P_{\text{out}_1}(R_1, \text{SNR})). \quad (10)$$

To compare the empirical throughput with the theoretical expectations, we develop Hybrid and Upper-bound methods utilizing MI outage probability. For each value of R_0 , R_1 , and SNR we compute and store the corresponding probabilities $P_{\text{out}_0}(R_0, \text{SNR})$ and $P'_{\text{out}_1}(R_1, \text{SNR})$. The Hybrid method (Algorithm 1) aims to identify the theoretical throughput that can be expected with the optimal MCS_0^* and MCS_1^* , chosen in Section VI-B:

$$T_{\text{tot,hybr}}(\text{SNR}) = T_{\text{tot}}(R_0^*(\text{SNR}), R_1^*(\text{SNR}), \text{SNR}), \quad (11)$$

where $R_0^*(\text{SNR}), R_1^*(\text{SNR}) = \underset{R_0, R_1}{\text{argmax}} T_{\text{tot,sim}}(R_0, R_1, \text{SNR})$.

To provide an upper-bound for an empirical throughput, we develop Algorithm 2 where throughput (10) is computed for each possible MCS combination (not only optimal), and for each SNR value the maximum value of $T_{\text{tot,up-b}}$ is identified:

$$T_{\text{tot,up-b}}(\text{SNR}) = T_{\text{tot}}(R_{0,\text{MI}}^*(\text{SNR}), R_{1,\text{MI}}^*(\text{SNR}), \text{SNR}), \quad (12)$$

where $R_{0,\text{MI}}^*(\text{SNR}), R_{1,\text{MI}}^*(\text{SNR}) = \underset{R_0, R_1}{\text{argmax}} T_{\text{tot}}(R_0, R_1, \text{SNR})$.

Fig. 8 illustrates the gap between the empirical throughput, throughput obtained via our Hybrid method, and upper-bound throughput. The throughput values $T_{\text{tot,sim}}^*$ and $T_{\text{tot,hybr}}$ are very close when the UE is in the low SNR regime and uses 16-16QAM or 16-64QAM. However, as soon as the receiver goes to the high SNR regime, where 64QAM is used, the gap between actual and predicted throughput increases. This can be explained by the fact that we model MI for the infinite codeblock length, while the codeblock length is in fact limited by the transport block size in a real LTE system.

VIII. CONCLUSION

We have presented a comparative study of the R-ML PIA and SIC receivers based on our implementation in the OAI simulator. Given a 5 MHz LTE bandwidth, the SIC receiver

Algorithm 1 Hybrid throughput $T_{\text{tot, hybr}}$

Input: SNR, R_0^* , R_1^* , $P_{\text{out}_0}(R_0, \text{SNR})$, $P_{\text{out}_1}(R_1, \text{SNR})$.**Output:** $T_{\text{tot, hybr}}(\text{SNR})$.

- 1: Given $R_0^*(\text{SNR})$, $R_1^*(\text{SNR}) = \underset{R_0, R_1}{\operatorname{argmax}} T_{\text{tot, sim}}(R_0, R_1, \text{SNR})$, find $P_{\text{out}_0}(R_0^*, \text{SNR})$ and $P_{\text{out}_1}(R_1^*, \text{SNR})$.
 - 2: To get $T_{\text{tot, hybr}}(R_0^*, R_1^*, \text{SNR})$, substitute $P_{\text{out}_0}(R_0^*, \text{SNR})$, $P_{\text{out}_1}(R_1^*, \text{SNR})$, R_0^* and R_1^* into (10).
-

Algorithm 2 Upper-Bound throughput $T_{\text{tot, up-b}}$

Input: SNR, $P_{\text{out}_0}(R_0, \text{SNR})$, $P_{\text{out}_1}(R_1, \text{SNR})$.**Output:** $T_{\text{tot, up-b}}(\text{SNR})$.

- 1: Find $R_{0, \text{MI}}^*(\text{SNR})$, $R_{1, \text{MI}}^*(\text{SNR}) = \underset{R_0, R_1}{\operatorname{argmax}} T_{\text{tot}}(R_0, R_1, \text{SNR})$.
 - 2: Substitute $R_{0, \text{MI}}^*(\text{SNR})$, $R_{1, \text{MI}}^*(\text{SNR})$, $P_{\text{out}_0}(R_{0, \text{MI}}^*(\text{SNR}), \text{SNR})$ and $P_{\text{out}_1}(R_{1, \text{MI}}^*(\text{SNR}), \text{SNR})$ into (10) to get $T_{\text{tot, up-b}}(\text{SNR}) = T_{\text{tot}}(R_{0, \text{MI}}^*(\text{SNR}), R_{1, \text{MI}}^*(\text{SNR}), \text{SNR})$.
-

outperforms the PIA receiver by 4 Mbit/s in Rician flat fading and 1.8 Mbit/s in Rayleigh flat fading. Moreover, the gains scale with the bandwidth. Our SIC receiver is 25% more time efficient than the PIA receiver, thanks to replacing the time consuming IA metric of the second CW with the SIC block. The signal processing time is less than 1.5 ms for 1 frame for both receivers, which makes our receivers suitable for real-time modems. The obtained findings will be extended to spatial multiplexing schemes of 5G New Radio.

APPENDIX

Derivation of Precoder Selection Algorithm

We aim to define the regions on the complex plane \mathbf{C} , where the correlation coefficient $\rho = \mathbf{h}_1^H \mathbf{h}_0$ guarantees

$$\frac{\|\mathbf{h}_0 + \mathbf{h}_1\|^2}{\|\mathbf{h}_0 - \mathbf{h}_1\|^2} \geq \frac{\|\mathbf{h}_0 + j\mathbf{h}_1\|^2}{\|\mathbf{h}_0 - j\mathbf{h}_1\|^2}. \quad (13)$$

Consider the complex vectors \mathbf{a} and \mathbf{b} , then

$$\|\mathbf{a} + \mathbf{b}\|^2 = (\mathbf{a} + \mathbf{b})^H (\mathbf{a} + \mathbf{b}) = \|\mathbf{a}\|^2 + \mathbf{a}^H \mathbf{b} + \mathbf{b}^H \mathbf{a} + \|\mathbf{b}\|^2.$$

Then the numerators and denominator can be rewritten as

$$\|\mathbf{h}_0 + \mathbf{h}_1\|^2 = \|\mathbf{h}_0\|^2 + \rho^* + \rho + \|\mathbf{h}_1\|^2, \quad (14)$$

$$\|\mathbf{h}_0 - \mathbf{h}_1\|^2 = \|\mathbf{h}_0\|^2 - \rho^* - \rho + \|\mathbf{h}_1\|^2, \quad (15)$$

$$\|\mathbf{h}_0 + j\mathbf{h}_1\|^2 = \|\mathbf{h}_0\|^2 + j\rho^* - j\rho + \|\mathbf{h}_1\|^2, \quad (16)$$

$$\|\mathbf{h}_0 - j\mathbf{h}_1\|^2 = \|\mathbf{h}_0\|^2 - j\rho^* + j\rho + \|\mathbf{h}_1\|^2. \quad (17)$$

Multiplying both parts of (13) with denominators $\|\mathbf{h}_0 - \mathbf{h}_1\|^2$ and $\|\mathbf{h}_0 - j\mathbf{h}_1\|^2$, we obtain

$$\|\mathbf{h}_0 + \mathbf{h}_1\|^2 \|\mathbf{h}_0 - j\mathbf{h}_1\|^2 \geq \|\mathbf{h}_0 + j\mathbf{h}_1\|^2 \|\mathbf{h}_0 - \mathbf{h}_1\|^2. \quad (18)$$

We further simplify

$$\|\mathbf{h}_0 + \mathbf{h}_1\|^2 (\rho^* + \rho + j\rho - j\rho^*) \geq 0, \quad (19)$$

where $\|\mathbf{h}_0 + \mathbf{h}_1\|^2$ is always non-negative, and thus

$$(\rho^* + \rho + j\rho - j\rho^*) \geq 0. \quad (20)$$

Decomposing ρ into real and imaginary parts, we have

$$\rho = \Re(\rho) + j\Im(\rho), \quad \rho^* = \Re(\rho) - j\Im(\rho).$$

Now (20) can be further developed as

$$\begin{aligned} & j(\Re(\rho) + j\Im(\rho) - \Re(\rho) + j\Im(\rho)) \\ & + \Re(\rho) - j\Im(\rho) + \Re(\rho) + j\Im(\rho) \geq 0 \\ \iff & \Re(\rho) \geq \Im(\rho) \end{aligned}$$

Thus, the inequality (13) is satisfied for any ρ such that $\Re(\rho) \geq \Im(\rho)$.

REFERENCES

- [1] 3GPP, "Network-assisted interference cancellation and suppression for lte," 3GPP, Tech. Rep. TR 36.866 v12.0.1 Release 12, March 2014.
- [2] E. N. Onggosanusi, A. G. Dabak, T. Schmidl, and T. Muharemovic, "Capacity analysis of frequency-selective mimo channels with sub-optimal detectors," in *2002 IEEE International Conference on Acoustics, Speech, and Signal Processing*, vol. 3, May 2002, pp. III-2369-III-2372.
- [3] G. Caire, G. Taricco, and E. Biglieri, "Bit-interleaved coded modulation," *IEEE Transactions on Information Theory*, vol. 44, no. 3, pp. 927-946, May 1998.
- [4] S. Aubert, M. Mohaisen, F. Nouvel, and K. Chang, "Parallel QR decomposition in LTE-A systems," in *2010 IEEE 11th International Workshop on Signal Processing Advances in Wireless Communications (SPAWC)*, June 2010, pp. 1-5.
- [5] R. Thomas, R. Knopp, B. Maharaj, and L. Cottatellucci, "Detection using block QR decomposition for MIMO hetnets," in *Signals, Systems and Computers, 2014 48th Asilomar Conference on*, Nov 2014, pp. 1291-1295.
- [6] R. Ghaffar and R. Knopp, "Low complexity metrics for bicm siso and MIMO systems," in *Vehicular Technology Conference (VTC 2010-Spring)*, 2010 IEEE 71st, May 2010, pp. 1-6.
- [7] H. Lee, J. H. Lim, S. Cho, and S. Kim, "Interference cancellation based on blindly-detected interference parameters for lte-advanced ue," in *2015 IEEE International Conference on Communications (ICC)*, June 2015, pp. 3143-3148.
- [8] R. Ghaffar and R. Knopp, "Linear precoders for multiuser mimo for finite constellations and a simplified receiver structure under controlled interference," in *2009 Conference Record of the Forty-Third Asilomar Conference on Signals, Systems and Computers*, Nov 2009, pp. 1431-1435.
- [9] S. Wagner and F. Kaltenberger, "Interference-aware receiver design for MU-MIMO in LTE: Real-time performance measurements," *Intel Technology Journal, Volume 18, N°1, 2014*, 01 2014.
- [10] E. Lukashova, F. Kaltenberger, R. Knopp, and C. Bonnet, "PHY layer abstraction for SU-MIMO LTE system employing parallel Interference-Aware detection," in *International Workshop on Link and System Level Simulations 2016 (IWSLS'16)*, Vienna, Austria, June 2016.
- [11] E. Lukashova, F. Kaltenberger, and R. Knopp, "Single-User MIMO ML successive interference canceling receiver with HARQ-IR protocol," in *21st International ITG Workshop on Smart Antennas (WSA 2017)*, Berlin, Germany, Mar. 2017.
- [12] "Openairinterface," 2017. [Online]. Available: <http://www.openairinterface.org/>
- [13] 3GPP, "Evolved universal terrestrial radio access (e-utra); physical layer procedures," 3GPP, Tech. Rep. Technical Specification 36.213 V13.0.0 Release 13, May 2016.
- [14] —, "Evolved universal terrestrial radio access (e-utra); physical channels and modulation," 3GPP, Tech. Rep. Technical Specification 36.211 V12.6.0 Release 12, July 2015.
- [15] —, "Evolved universal terrestrial radio access (e-utra); multiplexing and channel coding," 3GPP, Tech. Rep. Technical Specification 36.212-V12.7.0 Release 12, July 2015.
- [16] Z. Wang and G. B. Giannakis, "Outage mutual information of space-time mimo channels," *IEEE Transactions on Information Theory*, vol. 50, no. 4, pp. 657-662, April 2004.
- [17] S. Schwarz, C. Mehlh r, and M. Rupp, "Calculation of the spatial preprocessing and link adaption feedback for 3gpp umts/lte," in *2010 Wireless Advanced 2010*, June 2010, pp. 1-6.
- [18] R. Ghaffar and R. Knopp, "Making multiuser mimo work for lte," in *21st Annual IEEE International Symposium on Personal, Indoor and Mobile Radio Communications*, Sept 2010, pp. 625-628.